ABLE: An Automated Bacterial Load Estimator for the Urinoculture Screening

Paolo Andreini, Simone Bonechi, Monica Bianchini, Andrea Garzelli and Alessandro Mecocci
Department of Information Engineering and Mathematics, University of Siena, Via Roma 56, Siena, Italy

Keywords: Image Classification, Automatic Urinoculture Screening, Urinary Tract Infections.

Abstract: Urinary Tract Infections (UTIs) are very common in women, babies and the elderly. The most frequent cause is a bacterium, called Escherichia Coli, which usually lives in the digestive system and in the bowel. Infections can target the urethra, bladder or kidneys. Traditional analysis methods, based on human experts' evaluation, are typically used to diagnose UTIs, an error prone and lengthy process, whereas an early treatment of common pathologies is fundamental to prevent the infection spreading to kidneys. This paper presents an image based Automated Bacterial Load Estimator (ABLE) system for the urinoculture screening, that provides quick and traceable results for UTIs. Infections are accurately detected and the bacterial load is evaluated through image processing techniques. First, digital color images of the Petri dishes are automatically captured, and cleaned from noisily elements due to laboratory procedures, then specific spatial clustering algorithms are applied to isolate the colonies from the culture ground and, finally, an accurate evaluation of the infection severity is performed. A dataset of 499 urine samples has been used during the experiments and the obtained results are fully discussed. The ABLE system speeds up the analysis, grants repeatable results, contributes to the process standardization, and guarantees a significant cost reduction.

1 INTRODUCTION

Urinary Tract Infections (UTIs), together with those of the respiratory tract, are of great clinical relevance for the high frequency with which they are found in common medical practice and because of the complications arising therefrom. UTIs can target the urethra, bladder or kidneys and they are mainly caused by Gram–negative microorganisms, with a high prevalence of *Escherichia Coli* (E. Coli, 70%) — which usually lives in the digestive system and in the bowel —, even if clinical cases frequently occur where complicated infections are caused by Gram–positive or multi–resistant germs, on which the common antimicrobial agents are inevitably ineffective, leading to therapeutic failures.

The urinoculture is a screening test in the case of hospitalized patients and pregnant women. In the standard protocol, the urine sample is seeded on a Petri dish that holds a culture substrate, used to artificially recreate the environment required for the bacterial growth, and incubated at 37° C overnight. After the incubation, each dish must be examined by a human expert, adding some more time to the medical report output. This common situation significantly departs from the needs of clinicians to have results in quick time, to set a targeted therapy, avoiding the use of broad–spectrum antibiotics and improving the patient management[1]. Moreover, traditional analysis methods suffer from further problems, such as possible errors arising in the visual determination of the bacterial load — due to the skills and the expertise of the individual operator —, and difficulties in the traceability of samples and results (Ballabio et al., 2010).

Recently, significant improvements in biology and medicine applications and decision support systems (Berlin et al., 2006) have been obtained by using hybrid methods, based on a combination of advanced image processing techniques (Deserno, 2011; Belazzi et al., 2011), artificial intelligence tools (Agah, 2014; Heckerling et al., 2007; Bianchini et al., 2013), machine learning (Bandinelli et al., 2012), expert systems, fuzzy logic (Torres and Nieto, 2006), genetic algorithms, and Bayesian modelling (Dey et al., 2010). In particular, the development of automated tools for results assessment (screening systems) has attracted increasing research interest during the last decade, because of their higher repeatability, accuracy, reduced staff time (that are the main limiting factors of manual screening), and lower costs (Bourbeau and Lede-

[1]Rapid reporting is crucial, especially when pediatric patients are involved, since, in this case, the infection symptoms are not always specific, while it is urgent to decide if an antibiotic therapy is necessary or not and when to start it.

Andreini, P., Bonechi, S., Bianchini, M., Garzelli, A. and Mecocci, A.
ABLE: An Automated Bacterial Load Estimator for the Urinoculture Screening.
DOI: 10.5220/0005687005730580
In *Proceedings of the 5th International Conference on Pattern Recognition Applications and Methods (ICPRAM 2016)*, pages 573-580
ISBN: 978-989-758-173-1

boer, 2013). *Automated urinalysis devices improve the capacity of the laboratory to screen more samples, producing results in less time than by manual screening. Moreover, the redeployment and lower grading of staff with the increased turnover and speed of urine screening, gave economic advantages of automated screening over manual screening* (NHS Purchasing and Supply Agency, 2011).

Even if some interesting research has been carried out in recent years for the urinoculture screening (Andreini et al., 2015), tracing the state–of–the–art in image processing/AI solutions to the automatic analysis of Petri dishes is difficult, since published results are often related to subtle variations of the core problem (that ranges from the classification of the infection type to the evaluation of its severity), pertinent to various domains (from food and beverage safety to environmental control and specific clinical analyses (Ogawa et al., 2012; Clarke et al., 2010; Brugger et al., 2012; Wang, 2011; Chen and Zhang, 2009)), and based on different datasets.

In this paper, we propose a tool called ABLE (Automatic Bacterial Load Estimator), that provides a decision support system for biologists. The system automatically gets dish images from a color camera and, through a suitable preprocessing phase, removes the non relevant elements, due to laboratory procedures (such as labels and written text). Then, ABLE implements spatial clustering techniques to isolate the colonies from the culture ground, even in presence of ground disuniformities. Thereafter, using the information obtained thanks to the background removal, the system identifies the infected plates, also establishing their bacterial load. Finally, ABLE is capable to reveal the presence of multiple infections grown on the same dish, to alarm the analyst for contamination. The ABLE system allows a substantial speedup of the whole procedure, besides avoiding the continuous transition between sterile and external environments. The final outcomes are directly stored along with the related analysis records (the image, the type of infection — unique or multiple —, and the colony count). Data used during experiments have been provided by DIESSE Ricerche Srl, Siena. Preliminary experiments show very promising results.

The paper is organized as follows. In Section 2, the procedure adopted to remove the noisily elements from images is described. Section 3 presents the background subtraction system and the method used to decide if a sample is infected or not, to evaluate the bacterial load; the procedure for establishing the number of different infections contemporary grown on the same plate is also illustrated. Finally, Section 4 collects experimental results, whereas conclusions are drawn in Section 5.

2 PREPROCESSING

In general, the plate–handling process requires some ancillary data that are added on the plate after the urinoculture seeding procedure (for instance, a written text with the manufacturer name, a label for patients traceability, etc.). The plates, used in this work, contain written text on the background for the type of culture ground (Agar chromID CPS) and the bioMérieux trademark. Moreover, a label is pasted underneath with the patient name and a bar code (see Fig. 1). These elements negatively affect the classification process and must be removed. They have a fixed shape and dimension, but their position can change from image to image.

2.1 Written Text Removal

To remove the text, a first problem to be solved is its precise localization inside the image. We have used a template matching approach, based on a sample of the written text manually extracted from an almost empty plate (see Fig. 1). Being the text fixed, the manual operation needs to be performed only once, at the very beginning of the preprocessing phase (thereafter it is stored in the system). Gradient variations (based on Sobel filtering (Gonzalez and Woods, 2008) procedure) were evaluated to guarantee independence from light alterations.

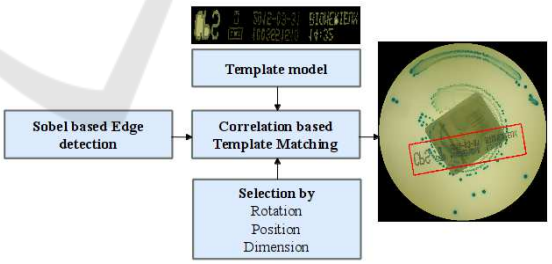

Figure 1: Written text removal scheme.

Normalized Cross Correlation (NCC) (Ahuja and Tuli, 2013) has been used to detect the text position:

$$R(x,y) = \frac{1}{n}\sum_{x,y}\frac{\left(f(x,y)-\overline{f}\right)\left(t(x,y)-\overline{t}\right)}{\sigma_f \sigma_t}$$

where n is the number of pixels in $t(x,y)$ (the template) and in $f(x,y)$ (the image), $\overline{f}$, σ_f, $\overline{t}$ and σ_t are, respectively, the average and the standard deviation of f and t. While the text appearance is fixed (and can be stored), its rotation is not, and must be compensated.

To this end, different rotated versions of the acquired template are applied to the image and the best match is selected. To speed up the process, the template search area is limited to a subpart of the whole image. In fact, the text printing process grants some tolerance limits to the positional variability (e.g., the distance between the text position and the image center cannot exceed a certain threshold).

2.2 Label Removal

The next preprocessing step aims at removing the area occupied by the label, attached under the plate. The image acquisition device uses back lighting, so that the light passes through the semi–transparent culture ground and the label, and the latter absorbs the most of the light. As a result, the label area is always darker than the surroundings. To segregate the label, we use an adaptive threshold obtained by applying the Otsu's method (Otsu, 1979) to the image luminance (Fig. 2 (b)). The binary mask gained after thresholding contains the darkest regions in the plate (some colonies and the label). A morphological opening is then used to regularize the mask shape, based on a circular structuring element, with a diameter slightly smaller than the shortest label side. In this way, bacterial colonies and other artifacts, smaller than the label, are removed (Fig. 2 (c)). Finally, the minimum perimeter rectangle of the largest connected component is computed, recovering the label position. Pixels belonging to this rectangle are disregarded during further processing steps. Moreover, the patients' name is blurred by applying a severe smoothing on some fixed positions relative to the detected label, in order to work without worrying about privacy issues (Fig. 2 (d)).

3 INFECTED PLATE DETECTION

The main requirement for ABLE has been that of correctly identifying positive samples. In general, the number of negative samples is greater than that of positive samples (more than 60% are negative results) (Broerm et al., 2011). Moreover, negative samples have small clinical relevance since, generally, they do not need further examination. So, for a biological laboratory, a highly accurate classification into positive and negative cases represents a large workload reduction. Usually, a plate can be considered positive if the number of microorganisms per milliliter of urine exceeds 10^5. Our dataset samples were seeded using a bioMérieux Previ Isola automated agar plate inoculation system. This device starts from a fixed point and circularly spreads the urine sample over the whole plate: more serious is the infection, the greater is the angle between the starting point and the last colony grown on the plate. If the angle is wider than 180 degrees, then the sample is considered to be positive (Rice and Baruch, 2009). To identify the spread–angle, the bacterial colonies must be segregated from the culture ground.

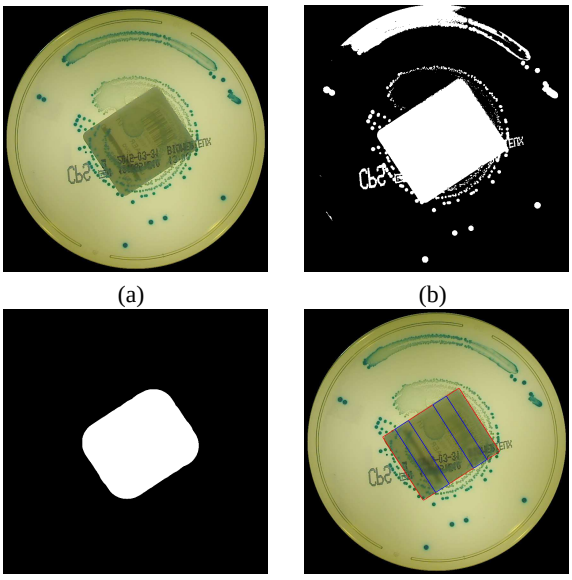

(a) (b) (c) (d)

Figure 2: In (a), the original image; in (b), the mask obtained with Otsu thresholding; in (c), the result of morphological opening; in (d), the red rectangle shows the label, and the blue rectangles show those parts that were blurred.

3.1 Color Space Analysis

Since a chromogenic medium is used as the ground seed, the pixel color is one of the most important feature to distinguish the bacterial colonies from the background. Therefore, preliminarily, the distribution of background colors has been analyzed in four different color spaces (i.e., RGB, HSV, CIE–Lab, and YCrCb). A supervised training procedure has been adopted, during which a human expert selected about 80 different regions belonging to the background and to the foreground. The same sample regions, extracted from a subset which was not employed in the testing phase, have been used also for training the Gaussian mixture models (see Sections 3.2 and 3.4). The chromatic components of the pixels belonging to such regions are accumulated to represent the typical background and foreground chromatic values. The Dunn's Index (*DI*) has been used to give a quantitative rank (based on the Centroid Linkage distance and the Centroid Diameter dispersion):

$$DI(X) = \frac{\min_{1\le i\le j\le k} d(C_i,C_j)}{\max_{1\le s\le k}\{\Delta(C_s)\}}$$

$$d(C_i,C_j) \triangleq \frac{1}{|C_i|+|C_j|}\left(\sum_{\vec{c}\in C_i} d(\vec{c},\mu_j) + \sum_{\vec{c}\in C_j} d(\vec{c},\mu_i)\right)$$

$$\mu_i \triangleq \frac{1}{|C_i|}\sum_{\vec{c}\in C_i}\vec{c}$$

$$\Delta(C_i) \triangleq \left(\frac{\sum_{\vec{c}\in C_i} d(\vec{c},\mu_i)}{|C_i|}\right)$$

where X represents the color space where DI is calculated, $\vec{c}$ is the chromatic vector of each pixel, k is the number of clusters, $d(C_i,C_j)$ is a dissimilarity function between two clusters C_i and C_j, $\Delta(C_i)$ is the mean distance of all the points from the mean, and μ_i is the mean of cluster i. DI is higher in the CIE–Lab space, which indicates a better clustering ability compared with the other color spaces. The same conclusion can be achieved by visually analyzing the color distribution in the four different spaces (Fig. 3).

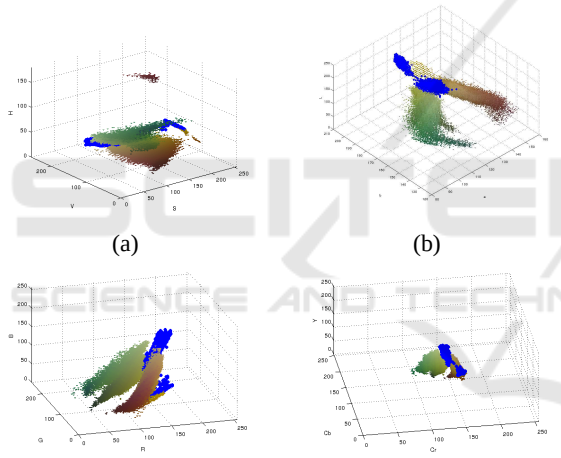

(a) (b) (c) (d)

Figure 3: Typical foreground elements are represented with their own colors, whereas the typical background color is plotted in blue. The scatter plots in (a), (b), (c) and (d) represent, respectively, the color distribution in the HSV, CIE–Lab, RGB and YCrCb color spaces.

3.2 Background Subtraction

Although the acquisition device uses a controlled illumination system, the effect of agar dishomogeneities, and of light disturbances from the external environment, produces relevant brightness variations in the background. Therefore, only the (a,b) chromatic components of the CIE–Lab color space have been used for detecting colonies, in order to gain a robust representation with respect to lighting changes, shadows and local variations. Moreover, the presence of some particular type of infections (Proteus Mirabilis) significantly changes the culture ground appearance (see Fig. 4). Consequently, the background clearly shows two different clusters in the CIE–Lab color space (as evidenced by the two blue areas in Fig. 3).

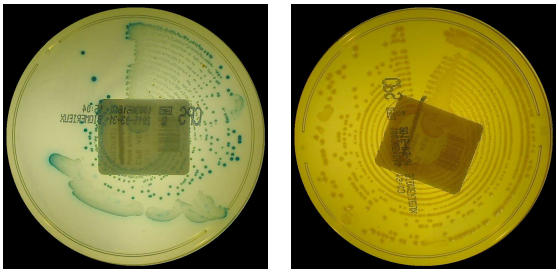

(a) (b)

Figure 4: In (a), the typical background color and, in (b), the background appearance changed by the Proteus Mirabilis infection.

By analyzing the background color samples by means of the Mardia and Henze–Zirkler normality tests (Mardia, 1970; Henze and Zirkler, 1990), it has become evident that a simple Gaussian model is unsuitable for modeling the two background clusters (see the contour lines of the background distributions in Fig. 5). This explains why a Gaussian mixture model (GMM) has been adopted to describe the corresponding multimodal density functions:

$$p(\theta) = \sum_{i=1}^{K} \Phi_i N(\mu_i,\Sigma_i)$$

where $\theta = (\vec{\mu},\vec{\Sigma})$ collects the mixtures parameters, whereas the i–th vector component is characterized by a normal distribution with weight Φ_i, means μ_i and covariance matrix Σ_i. The number of mixture components has been empirically chosen by observing the data contour lines, while the Expectation–Maximization (EM) algorithm has been used to estimate the mixture parameters. In Fig. 5, the contour lines estimated by the model are compared with those obtained using the original data. A similar approach has been also applied to the infection detection problem, as explained in Section 3.4.

The background subtraction procedure is shown in Fig. 6; a Mean–Shift segmentation algorithm is used to compensate for local background dishomogeneities. For each segment, the (a,b) modal values are compared with the Gaussian mixture models and, if the posterior probability of the background is the greatest one, the corresponding segment is considered to be part of the culture ground. Some specific type of infections cannot be classified by using chromatic information only, because their color is very similar to the background. In this case, spatial features (i.e., obtained with edge detection techniques) must be used

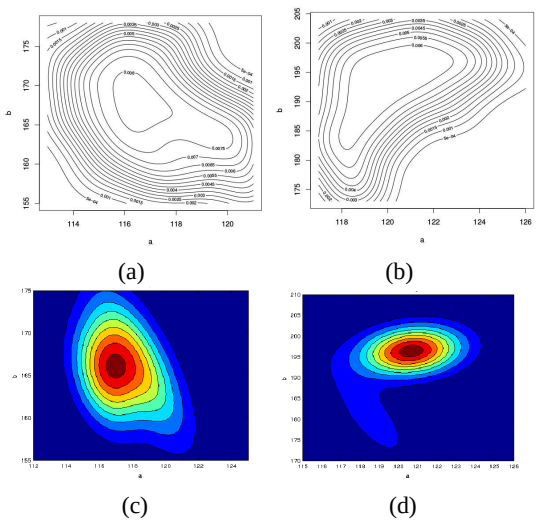

(a) (b) (c) (d)

Figure 5: In (a) and (b), the contour lines of the two background models; in (c) and (d), the contour lines estimated by the mixture model.

to obtain a suitable segmentation performance. In Fig. 7, some results are reported.

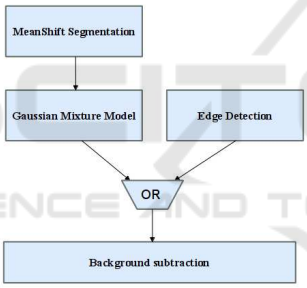

Figure 6: Background subtraction scheme.

3.3 Infection Severity Estimation

The angle between the inoculation starting point and the last colony found on the plate gives an indication of the infection severity. The plate image is divided into 64 equiangular sectors. For each sector, the foreground concentration is computed (number of foreground pixels divided by the total number of pixels in the sector). The sector with the maximum concentration is considered as that containing the inoculation starting point. From the starting sector, the image is analyzed counter–clockwise (opposite to the seeding direction) sector by sector, until a not empty sector is found. This last sector is considered as the colony proliferation end point. The angle between the starting point and the end point, in the clockwise direction, is used as a measure of the infection spread–angle over the plate. If the angle is wider than 180 degrees, the sample is considered as positive (infected).

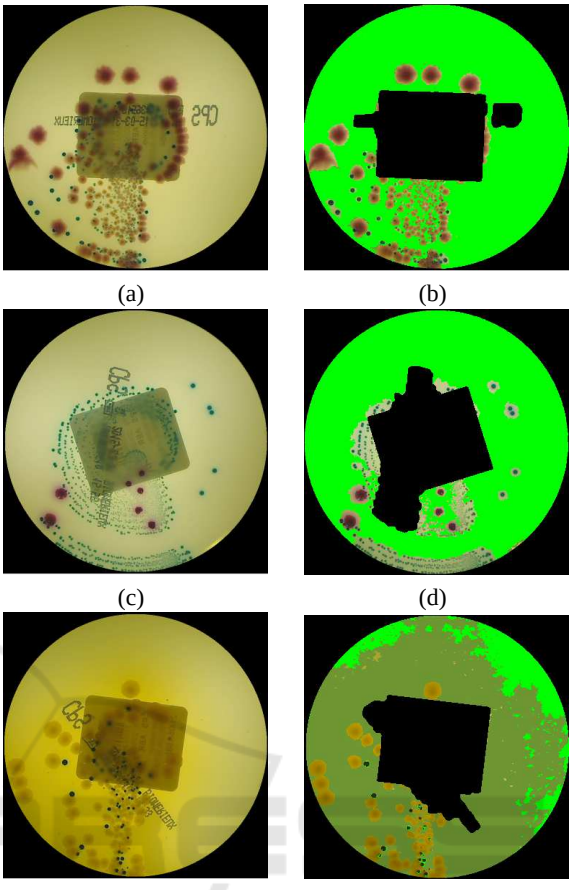

(a) (b) (c) (d) (e) (f)

Figure 7: In (a), (c), and (e), some original images; in (b), (d), and (f), the background subtraction results; the two background classes are respectively colored in green and dark green.

Unfortunately, our experiments clearly show that the spread–angle is not accurate enough to predict the infection severity. In fact, even if a colony spreads over the whole plate, some sectors within the spread–angle can be actually empty. To compensate this error, we simply subtract the angular contribution of the empty sectors from the estimate of the spread–angle. The algorithm is sketched in Fig. 8.

Moreover, further analyses have been carried out on the positive samples only, with the aim of distinguishing among severely infected plates ($\geq 10^6$) and moderately infected plates ($\geq 10^5$). To this aim, we estimate, one sector after the other, the ratio between the infected area and the sector area.

3.4 Detection of Multiple Infections

Biological laboratories daily examine a huge number of Petri plates. When a sample contains more than two infection strains, the plate needs further, specific,

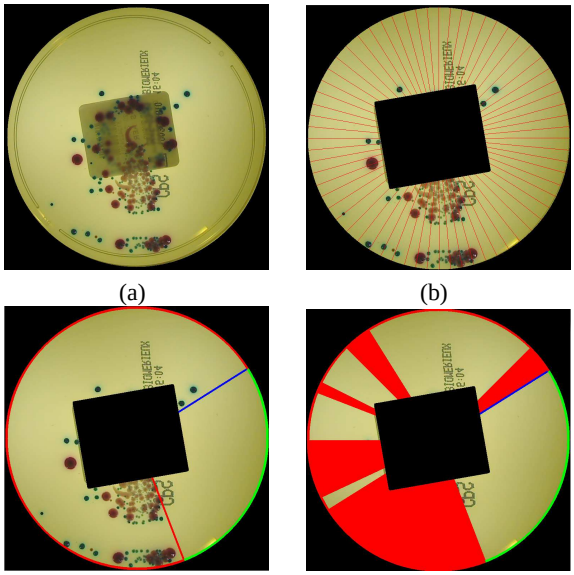

Figure 8: The original image (a) is divided in 64 sectors (b); in (c), the spread–angle is estimated and, in (d), only the not empty sectors (in red) are considered.

analysis. Therefore, it is important to quickly detect the presence of multiple infected plates where every type of infection is significantly present. Our proposed algorithm aims at detecting the following infection classes: E. Coli, Enterococcus Faecalis, KES group, Proteus, Pseudomonas Aeruginosa, and Morganella. The last three classes are not well represented within the dataset and, therefore, since they all produce yellow colonies, we decided to group them together in a "yellow infection" pseudo–class. When more than two classes are contemporary detected on the same plate, the sample has to be considered as "contaminated". To this end, the CIE–Lab (a,b) values of the four classes (E. Coli, Enterococcus Faecalis, KES group, yellow class) have been extracted, using some foreground samples collected during the initial color space analysis phase. As for the background subtraction module, only the chromatic components have been used. Again, the Mardia and Henze–Zirkler normality tests indicate that simple Gaussian models are unsuitable. The contour lines of each distribution are shown in Fig. 9.

As for the background subtraction module, a Gaussian mixture model (GMM) has been used to describe the various probability density functions. After the background subtraction, a Mean–Shift segmentation algorithm was applied in order to compensate for local dishomogeneities. For each segment, the (a,b) modal values are compared with the Gaussian mixture models of all the classes, and the maximum posterior probability gives the classifier output. It has

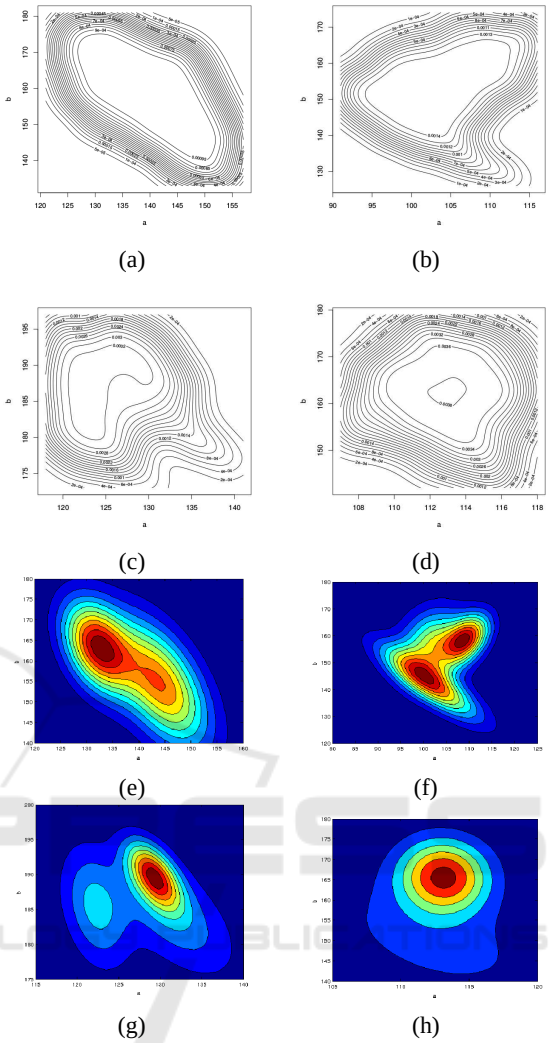

Figure 9: In (a), (b), (c) and (d), the contour lines, and in (e), (f), (g) and (h), the lines estimated with the mixture model respectively for E. Coli, E. Faecalis, the "yellow class", and KES.

been noted that, sometimes, there are halo–regions surrounding colonies. These halo–regions actually belong to the background but, in some cases, the presence of groups of nearby colonies changes the background appearance, producing some errors in the classification output. Moreover, when different types of infections, with different colors, overlap on the same plate, their color changes in the melding region, and this also leads to incorrect classifications. Since the unpredictable colors produced in these regions do not belong to any previously defined model, the posterior probability in those areas is likely to be low. To improve the performance in such situations, low values of the posterior probability are used to identify the uncertainty areas on the plate (see Fig. 10). The actual number of infections is determined with respect

to only those regions with a well–defined color.

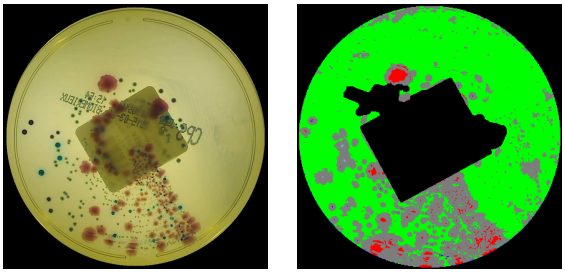

(a) (b)

Figure 10: In (a), the original image; in (b), in gray, the uncertainty region, in green, the background, in red, blue, dark blue and yellow the various infections.

4 RESULTS

The preprocessing algorithms have been tested on the whole data set comprised of 499 images. Overall, written texts have been correctly identified in the 86,78% of the images (433/499). However, it must be noted that the actual performance depends on the level of clutter in each plate. In the case of infected plates, a relevant part of the visual area is covered by the infection and the text is only partially visible (see Fig. 11). As a result, in infected images, the correct text detection rate is 75,45% (160/212), whereas in non infected images it is 95,12% (273/287).

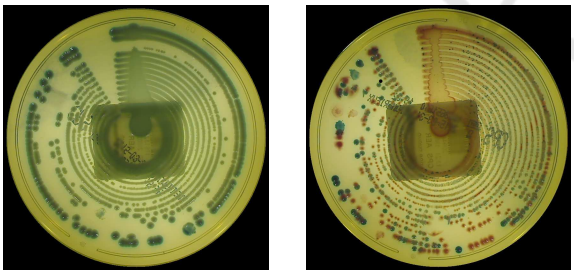

Figure 11: Two examples of highly infected plates, where the written text is significantly occluded.

It is worth noting, from a practical point of view, the text detection is not important for highly infected plates, because the infection severity mainly depends on how much the colony is spread on the plate, and the eventual few undetected text pixels do not influence the automatic classification results. The label removal algorithm also shows very good results: 100% of the whole dataset of 499 images has been correctly processed.

After the preprocessing phase, the system performs the infection severity estimation. The performance obtained by applying the procedure described in Section 3.3 to our dataset (accuracy and confusion matrix[2]) are reported in Table 1. As we can see, 22 images were incorrectly classified. However, it is important to note that these images are all false positive, so that we obtain a sensitivity of 100%. In fact, in our dataset, a positive sample is never confused with a negative one (false negative). This is a very desirable result, since a false positive "only" requires a further analysis by the human expert, whereas a false negative could lead to ignore the infection and to expose the patient to possible risks.

Table 1: Accuracy and confusion matrix obtained by ABLE.

Number of images	499
Correctly classified	477
Incorrectly classified	22
Accuracy	95,4%

Confusion Matrix	
Positive	Negative
212	22
0	265

For the 212 positive samples in our dataset — to be distinguished between severely infected ($\geq 10^6$) and moderately infected ($\geq 10^5$) — the obtained results are shown in Table 2. Although the classification accuracy was not astonishing, we can assert that, in almost all the cases in which ABLE fails, also the judgments of the human experts (three biologists, in this case) are mostly discordant.

Table 2: Classification accuracy for infected plates ($\geq 10^6$ vs. $\geq 10^5$), and confusion matrix, obtained by ABLE.

Number of images	212
Correctly classified	176
Incorrectly classified	36
Accuracy	83,01%

Confusion Matrix	
$\geq 10^5$	$\geq 10^6$
57	8
28	119

Even if the experimental results are actually very promising, they are devised on a small set of data, whereas the ABLE system must be experienced in

[2]A confusion matrix allows the visualization of the performance of a supervised learning classifier. Each column represents the instances in the predicted class, while each row represents the instances in the actual class. Its name stems from the fact that it clearly shows if the system is confusing two classes (i.e. commonly mislabeling one as another).

the daily practice of an analysis laboratory. To this aim, currently, ABLE is being extensively (and successfully) tested in DIESSE research laboratories, in order to compare its responses with those of a team of expert biologists, who are expected to evidence possible weaknesses to be solved before its final release.

5 CONCLUSIONS

Urinary tract infections can be caused by diverse microbes, including fungi, viruses, and bacteria. Bacteria are actually the most common cause of UTIs. Normally, bacteria that enter the urinary tract are rapidly removed by the body before they cause symptoms. However, sometimes bacteria overcome the bodys' natural defenses and, actually, roughly 150 millions of infections occur annually worldwide. In this paper, an automatic tool, called ABLE, to detect UTIs and to establish their severity, was described. The system shows a good accuracy in finding typical microorganisms present in humans, and gives no false negatives. Moreover, it is capable to reveal contaminated plates (where multiple infections are present on the same dish). Preliminary promising experimental results have been reported by DIESSE biologists, who are testing ABLE in their laboratories.

REFERENCES

Agah, A., editor (2014). *Artificial Intelligence in Healthcare*. CRC Press.

Ahuja, K. and Tuli, P. (2013). Object recognition by template matching using correlations and phase angle method. *International Journal of Advanced Research in Computer and Communication Engineering*, 2(3):1368–1373.

Andreini, P., Bonechi, S., Bianchini, M., Mecocci, A., and Di Massa, V. (2015). Automatic image classification for the urinoculture screening. In *Smart Innovation, Systems and Technologies*, volume Intelligent Decision Technologies, 39, pages 31–42.

Ballabio, C., Venturi, N., Scala, M. R., Mocarelli, P., and Brambilla, P. (2010). Evaluation of an automated method for urinoculture screening. *Microbiologia Medica*, 5(3):178–180.

Bandinelli, N., Bianchini, M., and Scarselli, F. (2012). Learning long–term dependencies using layered graph neural networks. In *Proceedings of IJCNN–WCCI 2012*, pages 1–8.

Belazzi, R., Diomidous, M., Sarkar, I. N., Takabayashi, K., Ziegler, A., McCray, A. T., and Sim, I. (2011). Data analysis and data mining: Current issues in biomedical informatics support systems. *Methods Inf. Med.*, 50(6):536–544.

Berlin, A., Sorani, M., and Sim, I. (2006). A taxonomic description of computer–based clinical decision support systems. *J. Biomedical Informatics*, 39:657–667.

Bianchini, M., Maggini, M., and Jain, L. C., editors (2013). *Handbook on Neural Information Processing*, volume Intelligent Systems Reference Library, 49. Springer.

Bourbeau, P. P. and Ledeboer, N. A. (2013). Automation in clinical microbiology. *Journal of Clinical Microbiology*, 51(6):1658–1665.

Broerm, M. A., Bahçeci, S., Vader, H. L., and Arents, N. L. (2011). Screening for urinary tract infections with the sysmex uf–1000i, urine flow cytometer. *Journal of Clinical Microbiology*, 49:1025–1029.

Brugger, S. D., Baumberger, C., Jost, M., Jenni, W., Brugger, U., and Múhlemann, K. (2012). Automated counting of bacterial colony forming units on Agar plates. *PLoS ONE*, 7(3):e33695.

Chen, W.-B. and Zhang, C. (2009). An automated bacterial colony counting and classification system. *Inf. Syst. Front.*, 11(4):349–368.

Clarke, M. L., Burton, R. L., Hill, A. N., Litorja, M., Nahm, M. H., and Hwang, J. (2010). Low–cost, high–throughput, automated counting of bacterial colonies. *Cytometry Part A*, 77(8):790–797.

Deserno, T. M., editor (2011). *Biomedical Image Processing*. Springer–Verlag, New York.

Dey, D. K., Ghosh, S., and Mallick, B. K. (2010). *Bayesian Modeling in Bioinformatics*. CRC Press.

Gonzalez, R. and Woods, R. (2008). *Digital Image Processing*. Addison Wesley.

Heckerling, P. S., Canaris, G. J., Flach, S. D., Tape, T. G., Wigton, R. S., and Gerber, B. S. (2007). Predictors of urinary tract infection based on artificial neural networks and genetic algorithms. *Int. J. Med. Inform.*, 76(4):289–296.

Henze, N. and Zirkler, B. (1990). A class of invariant consistent tests for multivariate normality. *Communications in Statistics – Theory and Methods*, 19(10):3595–3617.

Mardia, K. V. (1970). Measures of multivariate skewness and kurtosis with applications. *Biometrika*, 57(3):519–530.

NHS Purchasing and Supply Agency (2011). Automated urine screening systems.

Ogawa, H., Nasu, S., Takeshige, M., Funabashi, H., Saito, M., and Matsuoka, H. (2012). Noise–free accurate count of microbial colonies by time–lapse shadow image analysis. *Journal of Microbiological Methods*, 91(43):420–428.

Otsu, N. (1979). A threshold selection method from gray–level histograms. *IEEE Trans. Sys. Man Cyber.*, 9:62–66.

Rice, F. and Baruch, A. (2009). Evaluation of BioMérieuxs PREVI Isola, an automated microbiology specimen processor: Improving efficiency and quality of results.

Torres, A. and Nieto, J. J. (2006). Fuzzy logic in medicine and bioinformatics. *J. of Biomedicine and Biotechnology*, (91908).

Wang, W. (2011). Colony image acquisition system and segmentation algorithms. *Optical Engineering*, 50(12):123001–123010.